NJC

PAPER

Synthesis of BiVO₄ *via* oxidant peroxo-method: insights into the photocatalytic performance and degradation mechanism of pollutants†

Osmando F. Lopes,[ab] Kele T. G. Carvalho,[b] Gabriel K. Macedo,[c]
Vagner R. de Mendonça,[d] Waldir Avansi Jr.*[e] and Caue Ribeiro[b]

This paper reports the synthesis of monoclinic bismuth vanadate (BiVO₄) by the oxidant peroxide method with crystallization under hydrothermal conditions, and its catalytic performance on the photodegradation of pollutants under visible light. The as-synthesized BiVO₄ materials were characterized by means of X-ray diffraction (XRD), energy-dispersive X-ray spectroscopy (EDS), Raman spectroscopy, Ultraviolet-visible diffuse reflectance spectroscopy (UV-Vis DRS) and scanning electron microscopy (SEM). Hydrothermal treatment above 80 °C was required to obtain pure monoclinic BiVO₄ phase by releasing V^{5+} ions from vanadium peroxo complexes. With the increase in hydrothermal reaction temperature, the particle size decreased. All BiVO₄ samples presented large size and shape distribution and band gap of approximately 2.40 eV. The as-prepared BiVO₄ catalysts showed high photoactivity for decomposition of model pollutants, methylene blue (MB) and rhodamine B (RhB) dyes, under exposure to visible light. The photodegradation mechanism was evaluated by adding scavengers, DMSO and KBrO₃, which were used to probe •OH radical and conduction band (CB) electrons, respectively. It was observed that photodegradation of MB and RhB dyes is caused by the action of •OH radicals, and that BiVO₄ CB electrons do not have reduction potential sufficiently high to reduce dissolved oxygen to O_2^{-}•. It was proven that the indirect mechanism, *i.e.* •OH radical formation, plays the major role on the BiVO₄-assisted photodegradation process.

1. Introduction

Titanium dioxide (TiO₂)[1–6] and zinc oxide (ZnO)[7–10] are the main semiconductors applied in heterogeneous photocatalysis processes such as organic pollutants degradation and water splitting.[11,12] These materials possess specific characteristics that are regarded as crucial for good photocatalytic performance under UV-light when compared with other materials, such as band gap values of 3.2 eV

[a] *Departamento de Química, Universidade Federal de São Carlos-UFSCar, Rod. Washington Luiz, km 235, CEP 13565-905, São Carlos-SP, Brazil. E-mail: osmando_iq@hotmail.com*

[b] *Laboratório Nacional de Nanotecnologia para o Agronegócio (LNNA)-Embrapa Instrumentação, Rua XV de Novembro, 1452, CEP 13560-970, São Carlos-SP, Brazil. E-mail: kele_quimica@hotmail.com, caue.ribeiro@embrapa.br*

[c] *Instituto de Química de São Carlos, Universidade de São Paulo-USP, Av. Trabalhador São Carlense, 400, CEP 13560-970, São Carlos-SP, Brazil. E-mail: gabrielmacedo@iqsc.usp.br*

[d] *Instituto Federal de São Paulo, IFSP, Avenida João Olímpio de Oliveira, CEP 18202-000, Itapetininga-SP, Brazil. E-mail: vagneromito@yahoo.com.br*

[e] *Departamento de Física, Universidade Federal de São Carlos, Rod. Washington Luiz, km 235, CEP 13565-905, São Carlos-SP, Brazil. E-mail: w_avansi@yahoo.com.br*

† Electronic supplementary information (ESI) available. See DOI: 10.1039/c5nj00984g

and 3.4 eV, respectively, suitable textural properties, and slow recombination rate of a photogenerated electron–hole pair.[10,13] However, these materials can only be activated by UV radiation (wavelength below of 385 nm), which represents less than 5% of all solar energy that reaches the earth's surface, thereby eliminating their application under natural conditions.[14–19]

In this sense, semiconductors that can be activated by visible radiation have generated much scientific interest. Bismuth vanadate (BiVO₄) is a n-type semiconductor with band gap values ranging from 2.4 to 2.8 eV, depending on its crystalline phase.[20,21] BiVO₄ exists in three different crystalline phases: two tetragonal structures (zircon type and scheelite type), and one monoclinic structure (scheelite type). Among them, the monoclinic phase shows better photocatalytic performance under visible radiation, probably due to the lower and more suitable band gap of around 2.4 eV.[22–24] This low band gap value is a result of the hybridization between the Bi 2s orbital and the O 2p orbital, which causes a shift in the valence band, and decreases the difference of energy between the valence and conduction bands.[20,25] Although monoclinic BiVO₄ phase has been well studied as a photocatalyst, its role in the mechanism involved in the photocatalysis process is still open.

As a matter of fact, photocatalytic performance of semiconductors is also influenced by their structural, electronic and morphologic

characteristics, and the procedure used to synthesize them; these all have direct effects on their properties.[4,8,14,26–28] Several methods have been used to obtain photocatalysts: these include the sol–gel technique, polymeric precursor method, oxidant peroxide method (OPM), precipitation and co-precipitation.[20,29] Among these, the OPM method with crystallization under hydrothermal conditions is a remarkable route, since it possesses several advantages for the synthesis of nanostructures, especially low temperatures of crystallization, elimination of foreign ions or organic ligands, and control of morphology and structure of the semiconductor crystals through the synthesis parameters.[27,30,31]

Therefore, the aim of this study was to develop a new method to obtain monoclinic $BiVO_4$ at a low temperature, and to evaluate the photocatalytic performance of this semiconductor under visible light. The effect of the hydrothermal treatment on the structural, electronic, and morphologic properties of the $BiVO_4$ is described in this paper. Furthermore, we studied the major mechanism involved in the photodegradation of model pollutants by examining the behavior of different scavengers in the photocatalytic process, and by detection of hydroxyl radicals.

2. Experimental

2.1 Synthesis of $BiVO_4$

$BiVO_4$ samples were obtained using the oxidant peroxide method (OPM) followed by crystallization under hydrothermal conditions. First, 0.69 g of $Bi(NO_3)_3 \cdot 5H_2O$ (Vetec – Sigma) and 0.16 g of NH_4VO_3 (Vetec – Sigma) were added to 40 mL of distilled water under vigorous stirring, where the Bi : V molar ratio was kept at 1 : 1. Then, hydrogen peroxide (H_2O_2 30%, Synth) was added to the solution with H_2O_2 : M molar ratio equal to 10 : 1 (where M is the sum of Bi and V mols). The solution instantaneously presented a yellow color, which indicated formation of a vanadium peroxo complex.[31] This complex was crystallized for 12 hours using a homemade hydrothermal reactor, where the synthesis temperature was varied in a range between 80 °C and 160 °C. A synthesis at room temperature (25 °C) was also performed in order to understand the effect of the hydrothermal treatment on material crystallization. The samples were washed three times with distilled water, and subsequently with isopropyl alcohol, followed by centrifugation and then drying in an oven at 60 °C for 12 h. The sample obtained at room temperature was identified as BV-25, and the other samples were identified as BV-HTXX, where HT refers to "hydrothermal treatment" and XX is the synthesis temperature.

2.2 Powder characterization

Powder X-ray diffraction (XRD) was conducted using a Shimadzu XRD6000 diffractometer operating with Cu Kα radiation generated at 30 kV and a filament current of 30 mA. The 2θ range from 10 to 70° was continuously scanned with a speed of 1° min^{-1} and a step width of 0.02°. Raman spectroscopy measurements were performed with a FT-Raman spectrometer (Bruker RAM II with a Ge detector), equipped with a Nd:YAG laser with a wavelength centered at 1064 nm. Ultraviolet-visible diffuse reflectance spectroscopy (DRS) was carried out with a Cary 5G spectrometer in the total reflection

mode with an integration cell and a scanned wavelength range of 200–800 nm.

A field emission gun scanning electron microscope (FEG-SEM Jeol JSM 6701F) working at 5 kV was used to verify the material's morphology. Semi-quantitative atomic compositions were evaluated by energy-dispersive X-ray spectroscopy (EDS) using a Thermo Noran device coupled to a SEM (Jeol JEM 2010).

The analysis of N_2 adsorption at 77 K was conducted in a Micrometrics ASAP 2000, and the specific surface area (SSA) was obtained by the application of BET modeling. Before these analyses, the samples were pre-treated (degasification) by heating at 80 °C under vacuum until reaching a degassing pressure of less than 10 μm Hg.

2.3 Photocatalytic properties and mechanism evaluation

The photocatalytic activity of the as-synthesized $BiVO_4$ samples was evaluated by studying the photodegradation of methylene blue (MB) dye, which is considered one of the most common chemicals used in industrial processes, and often causes environmental pollution.[5,26] In order to perform the photocatalysis experiments, 10 mg of the as-synthesized sample was added to 20 mL of a 5 mg L^{-1} MB aqueous solution. All experiments were performed at pH = 6.5. The as-prepared dispersions were stirred and exposed to visible light radiation in a homemade photo-reactor with six fluorescent lamps (Osram, 15 W and maximum intensity at 440 nm) operating at 18 °C. The representative image of the photo-reactor is shown in Fig. S1 (ESI†). The MB photodegradation was monitored by its absorption maximum at 665 nm at regular periods of time using a UV-Vis spectrophotometer (Shimadzu – 1601PC) in the absorbance mode. In order to reach adsorption equilibrium the samples were previously kept in contact with the MB dye solution for 12 h in the dark. For comparative purposes, the photocatalytic behavior of a pristine commercial tetragonal Bi_2O_3 phase (Sigma-Aldrich, nanopowders 200 nm) was also evaluated. The crystalline phase, particle size, and morphology of Bi_2O_3 were confirmed by XRD and FEG-SEM (Fig. S2 and S4, respectively, for ESI†). DRS spectra were obtained to answer the question of suitability of Bi_2O_3 as a reference compound under visible light (see Fig. S3, in ESI†). The tetragonal Bi_2O_3 phase presented a band gap of 2.48 eV, as expected.[32] Therefore, the Bi_2O_3 used as a reference compound in this work absorbs photons at similar energies when compared with as-synthesized $BiVO_4$ samples. So, a tetragonal Bi_2O_3 phase is a suitable photocatalyst for use as a reference in the photocatalytic process under visible light.

Two different methods were used to investigate the MB photodegradation mechanism catalyzed by $BiVO_4$. The first consisted of adding reactive species scavengers directly to the $BiVO_4$-containing MB solutions. In this procedure, dimethyl sulfoxide (DMSO) and potassium bromate ($KBrO_3$) were added as scavengers for •OH radicals and CB electrons, respectively.[33] The second method consisted of indirectly detecting •OH radicals employing the technique described by Ishibashi et al. (2000),[34,35] in which alkaline terephthalic acid (TA) solution, instead of MB solution, is mixed with $BiVO_4$ in the photo-reactor. TA readily reacts with •OH and forms a highly fluorescent product, 2-hydroxyterephthalic acid. This product has a

fluorescence emission at around 425 nm, and its amount is proportional to the amount of •OH radicals formed during the photocatalytic process.[31] The concentration of TA was set at 5×10^{-4} mol L^{-1} in a dilute NaOH (2×10^{-3} mol L^{-1}) solution.[31] At regular time intervals, aliquots of the suspension were collected and analyzed in a LS 50B fluorescence spectrometer (PerkinElmer). The fluorescence emission spectra were obtained with an excitation wavelength of 315 nm.

3. Results and discussion

3.1 Characterization of the as-synthesized samples

The XRD patterns for the as-synthesized $BiVO_4$ samples are shown in Fig. 1. It is noted that the sample obtained without hydrothermal treatment (BV-25) presented a mixture of crystalline phases. The diffraction peaks were indexed as belonging to tetragonal $[Bi_6O_6(OH)_3](NO_3)_3 \cdot 1.5H_2O$ phase (JCPDS: 53-1038, highlighted for #) and vanadium hydrogen oxide ($H_{3.7}V_6O_{13}$) (JCPDS: 38-0008, highlighted for *). It was also observed that the BV-25 suspension maintained its yellow color (the same characteristic color of the vanadium peroxo-complex) even after synthesis and centrifugation, indicating that the V^{5+} ions were not completely released from the complex, and the $BiVO_4$ formation was incomplete.[36] Conversely, the XRD patterns for the samples synthesized by hydrothermal treatment under temperatures ranging from 80 °C to 160 °C (Fig. 1) were similar and presented well-defined peaks, which could be indexed as the pure monoclinic $BiVO_4$ crystalline phase (JCPDS – 83-1699). This is possibly explained by the fact that H_2O_2 reacts with V^{5+} ions forming the stable peroxo-complex under environmental conditions during relatively short periods of time.[36] Thus, the subsequent hydrothermal treatment, even when performed at 80 °C, provides sufficient energy to degrade the vanadium peroxo-complex, making all V^{5+} ions free to form the $BiVO_4$ structure. Therefore, XRD results clearly showed that the hydrothermal treatment has a fundamental role in the synthesis of pure monoclinic $BiVO_4$. Further increases in the temperature of hydrothermal treatment did not lead to any significant long range structural changes in the $BiVO_4$ samples.
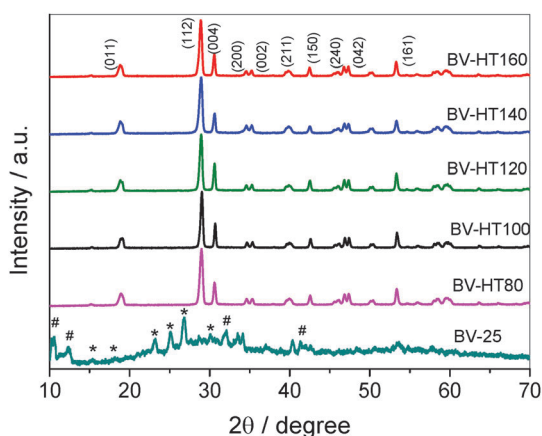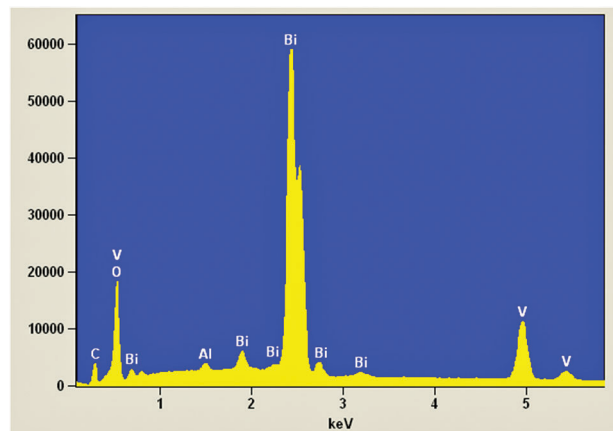

Fig. 2 EDS analysis of BV-25. The peaks related to O, Bi and V are identified in the plots.

Additionally, the semi-quantitative EDS analysis, performed on sample BV-25 (Fig. 2), confirmed the presence of only Bi and V elements with approximately 71% and 15% atomic percentages of Bi and V, respectively. This confirms that V^{5+} ions were not totally released at room temperature. The small peak below 0.5 keV and the peaks around 1.5 keV are related to the presence of carbon (C) from carbon conductive adhesive and the aluminum (Al) of stub, respectively.

Raman spectroscopy was performed in order to access medium-range order effects in the hydrothermally treated $BiVO_4$ samples, as seen in Fig. 3. The BV-HTXX samples, i.e. those obtained via hydrothermal treatment, presented similar spectra with five main Raman shifts at 120 cm^{-1}, 200 cm^{-1}, 330 cm^{-1}, 362 cm^{-1} and 826 cm^{-1}. The peaks at 120 cm^{-1} and 200 cm^{-1} are related to the external mode of $BiVO_4$; the peaks at 330 cm^{-1} and 362 cm^{-1} are ascribed to the asymmetric and symmetric deformation modes, respectively, of V–O bonds in the VO_4 tetrahedrons; and the peak at 826 cm^{-1} can be assigned to symmetric stretching of the V–O mode with A_g symmetry.[24,37] It was verified that these bands were not shifted as the temperature of the hydrothermal treatment was increased, meaning that no significant medium-range structural change occurred in the
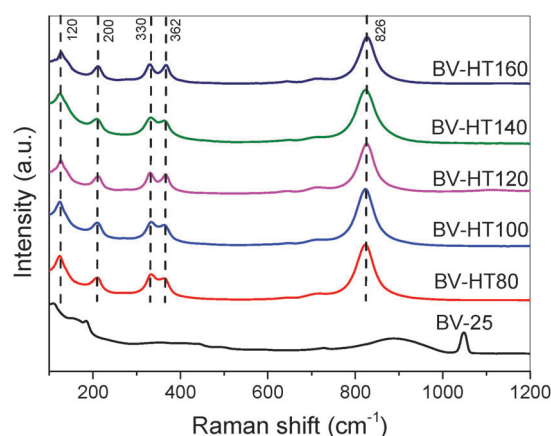

Fig. 1 Powder XRD patterns of as-synthesized $BiVO_4$ samples.

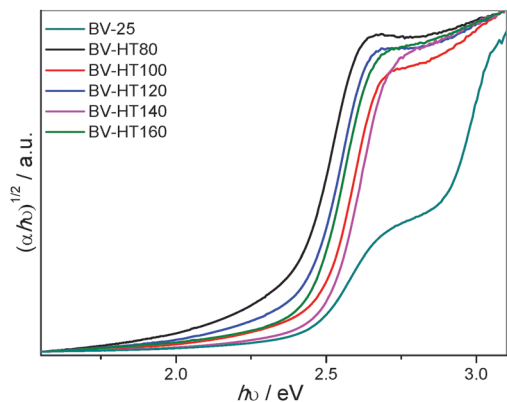Fig. 3 Raman scattering spectra of the as-synthesized $BiVO_4$ samples.

Fig. 4 Plots of $(\alpha h\nu)1/2$ *vs.* photon energy ($h\nu$) obtained by Tauc equation from DRS spectra.

Table 1 Band gap values of as-synthesized samples

Sample	Band gap/eV
BV-25	2.41/2.76
BV-HT80	2.35
BV-HT100	2.45
BV-HT120	2.40
BV-HT140	2.45
BV-HT160	2.40

BV-HTXX samples, and confirming the XRD results (Fig. 1). Furthermore, the BV-25 sample exhibited Raman scattering different from the BV-HTXX series, as expected.

The band gap values of the as-synthesized BiVO$_4$ samples were determined by applying the Tauc equation[38] to the diffuse reflectance spectroscopy UV-Vis data (Fig. 4). The band gap was calculated assuming that BiVO$_4$ has a direct-type transition, by plotting $(\alpha h\nu)^2$ *versus* $h\nu$.[20] The band gap values for the BiVO$_4$ samples exhibited small fluctuations, which ranged from 2.35 eV to 2.45 eV (Table 1), in a good agreement with literature values.[22,37]

Therefore, different temperatures of hydrothermal treatment did not induce any significant changes in electronic properties, allowing activation of the as-synthesized BiVO$_4$ samples by visible light. The BV-25 sample showed two distinct band gaps of 2.41 eV and 2.76 eV, highlighting the presence of two different crystalline phases, as observed by XRD and Raman scattering.

The morphology of the BiVO$_4$ samples was examined by FEG-SEM, and representative images are presented in Fig. 5. The BV-25 sample displayed irregular micrometric particles with different sizes, while for the BV-HT80 sample well faceted particles, also with different sizes and shapes, can be noted. On the other hand, for the BV-HT100 sample it was possible to observe the presence of more elongated particle branched in two axes, the known fish-bone BiVO$_4$ morphology.[39] Further increase in temperature (120 °C, 140 °C, and 160 °C) led to smaller particles in relation to BV-HT100. Size distribution of the particles was estimated using the software Image Pro Plus, by counting an average of 200 particles in different images (Fig. S5, ESI†). An average size equal to 828 nm, 443 nm, and 561 nm for BV-HT120, BV-HT140, and BV-HT160 samples, respectively, was observed. Therefore, the sizes of BV-HT140
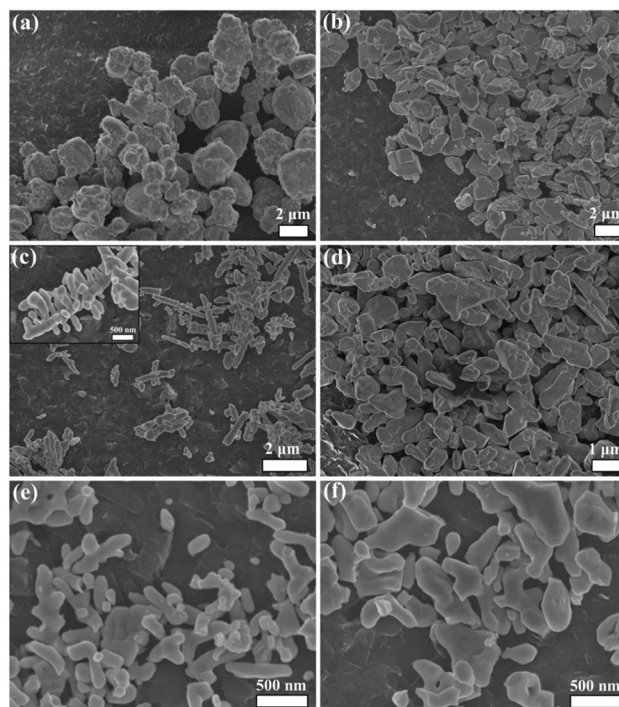

Fig. 5 Representative FEG-SEM images of (a) BV-25, (b) BV-HT80, (c) BV-HT100, (d) BV-HT120, (e) BV-HT140, and (f) BV-HT160. A magnification of a single particle is shown as an insert in (c).

and BV-HT160 are similar, since both distributions are wide but they present smaller sizes than BV-HT120. Despite the fact that the BV-HT120, BV-HT140, and BV-HT160 samples had a wide distribution of sizes, it is clear that increasing the temperature of the hydrothermal treatment decreases particles size of BiVO$_4$.[40]

3.2 Evaluation of photocatalytic properties

The photocatalytic properties of the as-synthesized samples were initially tested by using MB dye photodegradation induced by visible light (Fig. 6a). The commercial Bi$_2$O$_3$ nanopowder, employed as referential catalyst in the photocatalytic tests, presented lower photoactivity than all synthesized samples including that obtained at 25 °C. The direct photolysis of MB without catalyst was of approximately 8% after 3 h exposure to visible light. The BV-25 sample led to MB photodegradation of approximately 20%, and the MB photodegradation catalyzed for the BV-HTXX samples ranged from 40 to 50% (Fig. 6). These results confirm that the hydrothermal treatment step plays a fundamental role on the synthesis of highly efficient BiVO$_4$ photo-catalysts, since the BV-25 sample (mixed [Bi$_6$O$_6$(OH)$_3$](NO$_3$)$_3$·1.5H$_2$O and H$_{3.7}$V$_6$O$_{13}$ phases) presented the lowest photoactivity among all synthesized samples.

In order to test the reproducibility of the photocatalytic results, the experiments were performed in triplicate, and the first-order rate constant was calculated for each condition (Table 2). The R^2 values (higher than 0.97), confirm that the pollutant photo-degradation follows a first-order mechanism. It can be observed that there was no significant photocatalytic activity difference in the BV-HTXX series if the standard deviation is taken into account.
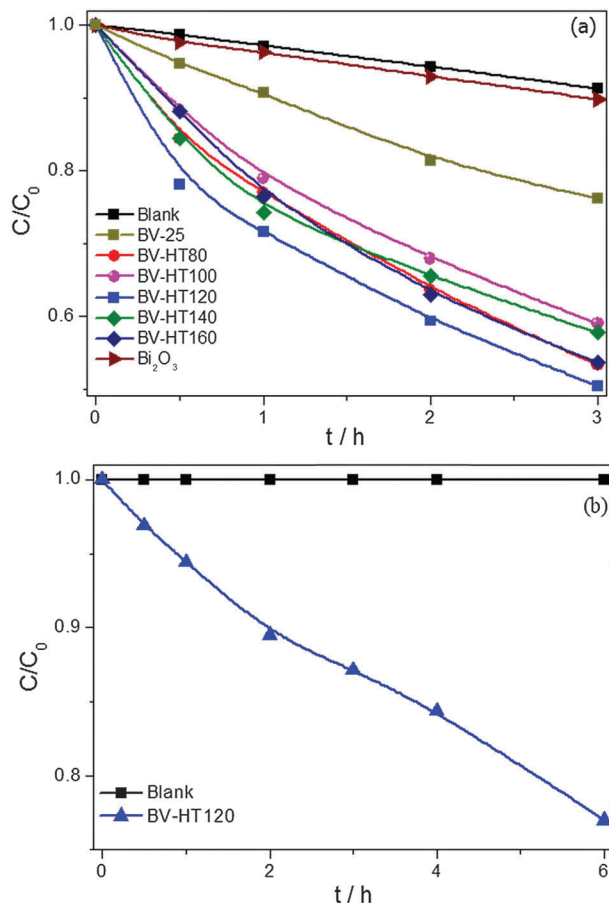
Fig. 6 (a) Photodegradation kinetics of MB dye (C_0 = 5 mg L^{-1}) catalyzed by BiVO$_4$ as a function of visible light exposure time; (b) photodegradation kinetic of RhB dye (C_0 = 5 mg L^{-1}) catalyzed by BV-HT120.

This result was expected, since the changes in temperature did not modify the features (structural, electronic, and morphologic) of the BiVO$_4$ samples. All synthesized BiVO$_4$ samples presented specific surface area (SSA) below of 1 m^2 g^{-1}, and any significant difference between samples was verified. Therefore, we considered that the temperature treatment has no significant influence in SSA, and consequently SSA does not play a fundamental role in this specific case. For the Bi$_2$O$_3$ samples (used as reference compound) the SSA presented a value equal to 2.8 m^2 g^{-1}. Despite the fact that the reference compound presented higher SSA compared to the as-synthesized samples, the performance in MB photodegradation of synthesized samples was significantly higher.

Table 2 First-order rate constants for the MB dye photodegradation reaction performed under visible radiation

Sample	$k \times 100$ (h^{-1})	R^2
Blank	0.3	0.998
BV-25	0.9 ± 0.1	0.980
BV-HT80	2.0 ± 0.2	0.980
BV-HT100	2.1 ± 0.3	0.970
BV-HT120	1.8 ± 0.3	0.970
BV-HT140	1.7 ± 0.2	0.970
BV-HT160	2.0 ± 0.2	0.986

Photoactivity of the BV-HTXX series was also examined for degradation of dyes with different physical–chemistry characteristics. The BV-HT120 sample (intermediate synthesis condition) was chosen as a representative sample in the study of RhB dye degradation under visible light (Fig. 6b). The result shown in Fig. 6b is remarkable, since the as-synthesized BiVO$_4$ presents activity for degradation of different organic pollutants. Even though BiVO$_4$ samples presented lower photoactivity for RhB dye photodegradation compared with MB dye, it's clear that the photoactivity can be improved by optimizing experimental conditions such as pH, ionic strength, and enhancement in dispersion by sonication.[26,41,42] Additional investigations in future works are necessary for optimization.

3.3 Photocatalytic mechanism study

The monoclinic BiVO$_4$ phase has been extensively studied for applications in photocatalysis,[14,40,43,44] but few studies were aimed at elucidating the mechanism involved in the photo-catalytic process. There are three principal mechanisms that may be involved in the catalyst-assisted photodegradation of pollutants: an indirect mechanism, a direct mechanism, and a photosensitization process.[5,31,45–49] Initially, we studied the photocatalytic mechanism by analyzing the effects of the addi-tion of two different reactive scavenger species to MB solutions during photocatalysis: KBrO$_3$ (strong oxidant, CB electrons acceptor) and DMSO (a $^\bullet$OH scavenger).[18,33] The representative BV-HT120 sample was used in these experiments, and the results are shown in Fig. 7a. Dissolved oxygen is considered to be a CB electrons scavenger that inhibits fast charge carrier recombination, and consequently formation of superoxide radical (O$_2$$^{-\bullet}$), which is very important for some photodegradation processes.[50] Therefore, a rational way of evaluating the importance of O$_2$$^{-\bullet}$ is to scavenge it with KBrO$_3$.[18,33] In this sense, if the photodegradation process is driven by O$_2$$^{-\bullet}$ radicals, the reaction rate is expected to be greatly decreased. On the other hand, if $^\bullet$OH radicals play the major role on the photodegradation process, then the reaction rate should be decreased in presence of excess DMSO.[18,33,51]

As it can be seen in Fig. 7a, the excess of KBrO$_3$ in MB solution caused a great increase in the photodegradation rate, from around 40% to 48% after 3 h of exposure to visible light (the rate constant underwent an increase of 25%). In order to check the effect of KBrO$_3$, blank experiments with and without KBrO$_3$ in MB dye solution (in absence of photocatalyst) were performed, where any effect in MB removal related to the KBrO$_3$ presence was verified. Thus, the effect of MB photodegradation was strictly related to electronic characteristics of the as-prepared photocatalyst. Two facts arose from this result. First, the O$_2$$^{-\bullet}$ radical has a negligible effect on the MB photodegradation mechanism (probably because the conduction band edge potential of BiVO$_4$ is not sufficiently high to reduce the dissolved oxygen), plus the irrelevant effect of the dye-photosensitized mechanism on MB photodegradation also was demonstrated.[52,53] The second fact is that a suitable CB electron acceptor, such as KBrO$_3$, can enhance the photoactivity of the BiVO$_4$ sample by inhibiting fast charge carrier recombination. Then different schemes to improve the
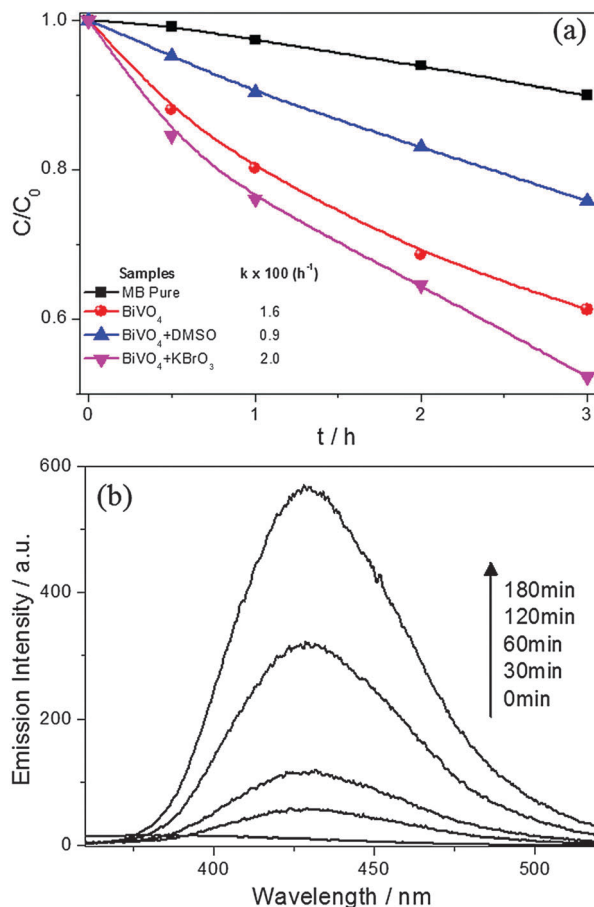
Fig. 7 (a) Photodegradation kinetic of MB dye (5 mg L^{-1}) catalyzed by BV-HT120 in the presence of KBrO$_3$ (scavenger of CB electrons) and DMSO (scavenger of •OH radicals). Kinetic rate constant values were added as an insert. (b) Spectral profile of 2-hydroxyterephthalic acid produced by BV-HT120, to detect radical •OH indirectly, as a function of visible light exposure time.

photocatalytic performance of the BiVO$_4$ samples can be performed, such as use of a sacrificial reagent (*e.g.*, Ag$^+$ and Au^{3+} cations) to scavenge CB electrons, and formation of heterostructures with metals and other suitable oxides.

The second scavenger, DMSO, can react quickly with •OH, forming a stable adduct, thus making the DMSO excess in MB solution capture all •OH radicals produced during the photocatalytic process.[51] As shown in Fig. 7a, the use of DMSO in excess considerably decreased the photodegradation rate from 40% to 25% after 3 h exposure (the rate constant underwent a decrease of 45%). Thus, it can be suggested that the indirect mechanism, *i.e.*, •OH radical generation has a major contribution for the MB dye photodegradation process.

In order to confirm the role played by •OH radicals in the photocatalytic mechanism, its detection was performed using terephthalic acid (TA) as a fluorescent probe.[34] The •OH radical is trapped by TA producing fluorescent 2-hydroxyterephthalic acid, as illustrated in Fig. 7b. Increases in the intensity of emission show that 2-hydroxyterephthalic acid was produced over time, proving that the BiVO$_4$ sample produced hydroxyl radicals. This confirms the results obtained with the DMSO
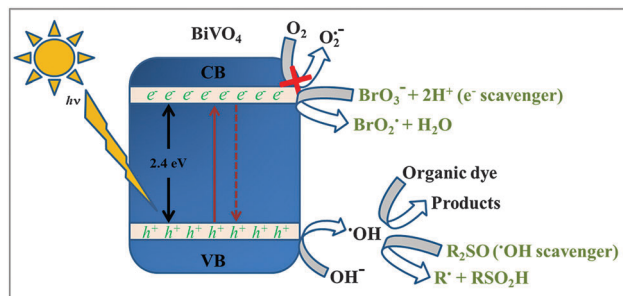

Fig. 8 Proposed mechanism for the photocatalytic reaction at the BiVO$_4$ photocatalyst surface in the absence or presence of scavengers.

scavenger, *i.e.*, the leading mechanism of MB dye photodegradation is based on hydroxyl radical attack. This finding was unexpected, since the generally proposed mechanisms of photodegradation reactions catalyzed by BiVO$_4$ are based mainly on O$_2$•$^-$ generation[54] and/or photosensitization.[46,47,55] According to our results, the mechanism of photodegradation for organic pollutants on the surface of BiVO$_4$ photocatalyst, in the absence or presence of scavengers, is schematically represented in Fig. 8.

4. Conclusions

In summary, the synthesis proposed in this work was efficient in obtaining monoclinic BiVO$_4$ at low temperatures. The as-prepared BiVO$_4$ displayed efficient photoactivity with the decomposition of model pollutants, methylene blue and rhodamine B dyes, under visible light. The hydrothermal treatment was required to release V^{5+} ions from vanadium peroxo complexes, forming a monoclinic BiVO$_4$ phase with a band gap of around 2.40 eV. The addition of two different radical scavengers to MB solutions during photocatalysis showed that the indirect mechanism, *i.e.*, generation of •OH radicals, has an important contribution for the photodegradation process, and that BiVO$_4$ CB electrons do not have sufficient reduction potential to reduce dissolved oxygen to O$_2$$^-$•. It was proven that suitable schemes (use of sacrificial reagents and formation of heterostructures between metals and oxides with BiVO$_4$) enhance the BiVO$_4$ photocatalytic performance.

Acknowledgements

Notes and references

1 U. I. Gaya and A. H. Abdullah, *J. Photochem. Photobiol., C*, 2008, **9**, 1–12.
2 M. R. Hoffmann, S. T. Martin, W. Choi and D. W. Bahnemann, *Chem. Rev.*, 1995, **95**, 69–96.
3 M. Fox and M. Dulay, *Chem. Rev.*, 1993, **93**, 341–357.

4 V. R. de Mendonça and C. Ribeiro, *Appl. Catal., B*, 2011, **105**, 298–305.

5 V. R. de Mendonça, O. F. Lopes, R. P. Fregonesi, T. R. Giraldi and C. Ribeiro, *Appl. Surf. Sci.*, 2014, **298**, 182–191.

6 H. J. Fan, C. S. Lu, W. L. W. Lee, M. R. Chiou and C. C. Chen, *J. Hazard. Mater.*, 2011, **185**, 227–235.

7 N. Daneshvar, D. Salari and A. Khataee, *J. Photochem. Photobiol., A*, 2004, **162**, 317–322.

8 T. R. Giraldi, G. V. F. Santos, V. R. de Mendonca, C. Ribeiro and I. T. Weber, *Mater. Chem. Phys.*, 2012, **136**, 505–511.

9 T. M. Milao, V. R. de Mendonça, V. D. Araújo, W. Avansi, C. Ribeiro, E. Longo and M. I. Bernardi, *Sci. Adv. Mater.*, 2012, **4**, 54–60.

10 S. G. Kumar and K. S. R. K. Rao, *RSC Adv.*, 2014, **5**, 3306–3351.

11 K. Maeda, *J. Photochem. Photobiol., C*, 2011, **12**, 237–268.

12 J. Yu, L. Qi and M. Jaroniec, *J. Phys. Chem. C*, 2010, 13118–13125.

13 M. A. Henderson, *Surf. Sci. Rep.*, 2011, **66**, 185–297.

14 J. Yu and A. Kudo, *Adv. Funct. Mater.*, 2006, **16**, 2163–2169.

15 D. Chatterjee and S. Dasgupta, *J. Photochem. Photobiol., C*, 2005, **6**, 186–205.

16 J. S. Jang, H. G. Kim and J. S. Lee, *Catal. Today*, 2012, **185**, 270–277.

17 G. B. Soares, B. Bravin, C. M. P. Vaz and C. Ribeiro, *Appl. Catal., B*, 2011, **106**, 287–294.

18 J. Cao, B. Xu, B. Luo, H. Lin and S. Chen, *Catal. Commun.*, 2011, **13**, 63–68.

19 H. Tong, S. Ouyang, Y. Bi, N. Umezawa, M. Oshikiri and J. Ye, *Adv. Mater.*, 2012, **24**, 229–251.

20 Y. Park, K. J. McDonald and K.-S. Choi, *Chem. Soc. Rev.*, 2013, **42**, 2321–2337.

21 X. Zhang, L. Du, H. Wang, X. Dong, X. Zhang, C. Ma and H. Ma, *Microporous Mesoporous Mater.*, 2013, **173**, 175–180.

22 S. Obregón, A. Caballero and G. Colón, *Appl. Catal., B*, 2012, **117–118**, 59–66.

23 Y. Zhang, G. Li, X. Yang, H. Yang, Z. Lu and R. Chen, *J. Alloys Compd.*, 2013, **551**, 544–550.

24 Y. Guo, X. Yang, F. Ma, K. Li, L. Xu, X. Yuan and Y. Guo, *Appl. Surf. Sci.*, 2010, **256**, 2215–2222.

25 J. Yang, D. Wang, X. Zhou and C. Li, *Chem. – Eur. J.*, 2013, **19**, 1320–1326.

26 H. A. J. L. Mourão, O. F. Lopes, C. Ribeiro and V. R. Mastelaro, *Mater. Sci. Semicond. Process.*, 2015, **30**, 651–657.

27 I. A. de Castro, W. Avansi and C. Ribeiro, *CrystEngComm*, 2014, **16**, 1514.

28 L. S. Cavalcante, J. C. Sczancoski, N. C. Batista, E. Longo, J. A. Varela and M. O. Orlandi, *Adv. Powder Technol.*, 2013, **24**, 344–353.

29 H. A. J. L. Mourão, V. R. de Mendonça, A. R. Malagutti and C. Ribeiro, *Quim. Nova*, 2009, **32**, 2181–2190.

30 J.-Y. Piquemal, E. Briot and J.-M. Brégeault, *Dalton Trans.*, 2013, **42**, 29–45.

31 O. F. Lopes, E. C. Paris and C. Ribeiro, *Appl. Catal., B*, 2014, **144**, 800–808.

32 H. Cheng, B. Huang, J. Lu, Z. Wang, B. Xu, X. Qin, X. Zhang and Y. Dai, *Phys. Chem. Chem. Phys.*, 2010, **12**, 15468–15475.

33 Y. Li, J. Wang, H. Yao, L. Dang and Z. Li, *J. Mol. Catal. A: Chem.*, 2011, **334**, 116–122.

34 K. Ishibashi and A. Fujishima, *J. Photochem. Photobiol., A*, 2000, **134**, 139–142.

35 K. Ishibashi and A. Fujishima, *Electrochem. Commun.*, 2000, **2**, 207–210.

36 W. Avansi, C. Ribeiro, E. R. Leite and V. R. Mastelaro, *Cryst. Growth Des.*, 2009, **9**, 3626–3631.

37 S. Obregón and G. Colón, *J. Mol. Catal. A: Chem.*, 2013, **376**, 40–47.

38 A. B. Murphy, *Sol. Energy Mater. Sol. Cells*, 2007, **91**, 1326–1337.

39 X. Lin, H. Li, L. Yu, H. Zhao, Y. Yan, C. Liu and H. Zhai, *Mater. Res. Bull.*, 2013, **48**, 4424–4429.

40 X. Zhang, Z. Ai, F. Jia, L. Zhang, X. Fan and Z. Zou, *Mater. Chem. Phys.*, 2007, **103**, 162–167.

41 A. G. S. Prado, L. B. Bolzon, C. P. Pedroso, A. O. Moura and L. L. Costa, *Appl. Catal., B*, 2008, **82**, 219–224.

42 L. S. Cavalcante, F. M. C. Batista, M. a. P. Almeida, a. C. Rabelo, I. C. Nogueira, N. C. Batista, J. A. Varela, M. R. M. C. Santos, E. Longo and M. Siu Li, *RSC Adv.*, 2012, **2**, 6438.

43 W. Liu, Y. Yu, L. Cao, G. Su, X. Liu, L. Zhang and Y. Wang, *J. Hazard. Mater.*, 2010, **181**, 1102–1108.

44 D. Ke, T. Peng, L. Ma, P. Cai and P. Jiang, *Appl. Catal., A*, 2008, **350**, 111–117.

45 O. F. Lopes, V. R. de Mendonça, F. B. F. Silva, E. C. Paris and C. Ribeiro, *Quim. Nova*, 2015, **38**, 106–117.

46 W. W. Lee, C.-S. Lu, C.-W. Chuang, Y.-J. Chen, J.-Y. Fu, C.-W. Siao and C.-C. Chen, *RSC Adv.*, 2015, **5**, 23450–23463.

47 Y.-R. Jiang, S.-Y. Chou, J.-L. Chang, S.-T. Huang, H.-P. Lin and C.-C. Chen, *RSC Adv.*, 2015, **5**, 30851–30860.

48 S.-T. Huang, Y.-R. Jiang, S.-Y. Chou, Y.-M. Dai and C.-C. Chen, *J. Mol. Catal. A: Chem.*, 2014, **391**, 105–120.

49 Y.-R. Jiang, H.-P. Lin, W.-H. Chung, Y.-M. Dai, W.-Y. Lin and C.-C. Chen, *J. Hazard. Mater.*, 2015, **283**, 787–805.

50 M. Yin, Z. Li, J. Kou and Z. Zou, *Environ. Sci. Technol.*, 2009, **43**, 8361–8366.

51 Y. Zhao, C. Eley, J. Hu, J. S. Foord, L. Ye, H. He and S. C. E. Tsang, *Angew. Chem., Int. Ed.*, 2012, **51**, 3846–3849.

52 W. Wang, X. Huang, S. Wu, Y. Zhou, L. Wang, H. Shi, Y. Liang and B. Zou, *Appl. Catal., B*, 2013, **134–135**, 293–301.

53 P. Chatchai, Y. Murakami, S. Kishioka, A. Y. Nosaka and Y. Nosaka, *Electrochim. Acta*, 2009, **54**, 1147–1152.

54 W. Wei, X. Yue, H. Cui, X. Lü and J. Xie, *J. Mater. Res.*, 2013, **28**, 3408–3416.

55 B.-X. Lei, P. Zhang, S.-N. Wang, Y. Li, G.-L. Huang and Z.-F. Sun, *Mater. Sci. Semicond. Process.*, 2015, **30**, 429–434.